AGU PUBLICATIONS

Geophysical Research Letters

RESEARCH LETTER
10.1002/2017GL074552

Key Points:
- We find that for certain time periods at the tops of simulated tropical cyclones, gradient wind balance has no physical solutions
- This invalidity is quantified using a nondimensional number (nonbalance index) which peaks during the intensification stages of the storms
- Lifetime-total values of nonbalance and intensification correlate; intensity during maximum nonbalance increases with nonbalance index

Supporting Information:
- Supporting Information S1
- Figure S1
- Table S1

Correspondence to:
Y. Cohen,
yairchn@caltech.edu

Citation:
Cohen, Y., N. Harnik, E. Heifetz, D. S. Nolan, D. Tao, and F. Zhang (2017), On the violation of gradient wind balance at the top of tropical cyclones, *Geophys. Res. Lett.*, *44*, 8017–8026, doi:10.1002/2017GL074552.

Received 12 JUN 2017
Accepted 17 JUL 2017
Accepted article online 20 JUL 2017
Published online 12 AUG 2017

On the violation of gradient wind balance at the top of tropical cyclones

Yair Cohen[1,2,3], Nili Harnik[1], Eyal Heifetz[1], David S. Nolan[4], Dandan Tao[5], and Fuqing Zhang[5]

[1]Department of Geosciences, Tel Aviv University, Tel Aviv, Israel, [2]Department of Environmental Sciences and Engineering, California Institute of Technology, Pasadena, California, USA, [3]Jet Propulsion Laboratory, California Institute of Technology, Pasadena, California, USA, [4]Rosenstiel School of Marine and Atmospheric Science, University of Miami, Coral Gables, Florida, USA, [5]Department of Meteorology and Atmospheric Science, Pennsylvania State University, University Park, Pennsylvania, USA

Abstract The existence of physical solutions for the gradient wind balance is examined at the top of 12 simulated tropical cyclones. The pressure field at the top of these storms, which depends on the vertically integrated effect of the warm core and the near surface low, is found to violate the gradient wind balance—termed here as a state of nonbalance. Using a toy model, it is shown that slight changes in the relative location and relative widths of the warm core drastically increase the isobaric curvature at the upper level pressure maps leading to nonbalance. While idealized storms return to balance within several days, simulations of real-world tropical cyclones retain a considerable degree of nonbalance throughout the model integration. Comparing mean and maximum values of different storms shows that peak nonbalance correlates with either peak intensity or intensification, implying the possible importance of nonbalance at upper levels for the near surface winds.

Plain Language Summary The assumption of a simple force balance (gradient wind balance) has served in idealized models for tropical cyclones in the past century. This assumption decouples the dynamics of the tropical cyclone's upper levels (15 km) from its surface winds. By examining the upper level of tropical cyclones in state of the art computer model, is it shown here that in certain scenarios the gradient wind balance has no physical validity at the top of tropical cyclones. This study motivates detailed upper level observations as well as new idealized theories.

1. Introduction

Idealized theories for the circulation that develops in tropical cyclones (TCs) as a response to the release of latent heat in the eyewall are based on the *balanced vortex model* [*Eliassen*, 1951; *Charney and Eliassen*, 1964; *Ooyama*, 1969; *Emanuel*, 1986; *Wirth and Dunkerton*, 2009]. This model combines the hydrostatic and the gradient wind balances (which together make thermal wind balance) with the radial momentum and thermodynamic equations. The assumption of gradient wind balance is motivated both by measurements [*Willoughby*, 1990] and by the requirement for balanced (and potentially predictable) flow at TC scale [*Ooyama*, 1982; *Raymond et al.*, 2015]. Given these assumptions, the balanced vortex model is able to describe the complexity of the coexisting horizontal and overturning circulations generated by heat and momentum sources, in a manner that is simple enough to be analytically solved. This model predicts that the tangential winds will peak at lower levels and decay upward [*Emanuel*, 1986; *Stern and Zhang*, 2016], conserving the value of the absolute angular momentum, which is set at the top of the boundary layer. Based on this model a wide range of theories have been presented for the steady structure and energetics [*Charney and Eliassen*, 1964; *Ooyama*, 1969; *Emanuel*, 1986], intensity [*Emanuel*, 1995], intensification [*Shapiro and Willoughby*, 1982; *Nolan et al.*, 2007], and existence of an eyewall [*Wirth and Dunkerton*, 2009].

In the balanced vortex model, the secondary circulation acts to exactly cancel the changes caused by eyewall heating and surface friction, maintaining thermal wind balance. Therefore, the upper level radial outflow is not directly driven by the radial pressure gradient and is considered as a passive component of the TC, serving only to evacuate mass from the core in exact balance with the low-level frictional inflow. Accordingly, most of the focus in previous studies and observational campaigns has been on air-sea interaction and the low-level primary circulation. In recent years, as part of continuing efforts to improve our

understanding of the TC intensification mechanism, much interest has been given to two relatively less explored components: warm-core structure and upper level dynamics.

The structure of the warm core (its height and the occasional existence of a double warm core) is considered an important aspect of the dynamics of a TC and is used operationally by the National Hurricane Center as an indication for the intensification of a storm or for upgrading a subtropical storm to a tropical storm [see, e.g., *National Hurricane Center*, 2010]. However, the mechanistic view of such a relation between the warm-core structure and TC intensity is still under debate. While some studies argue that the detailed structure of the warm core is related to TC intensity [*Ohno and Satoh*, 2015; *Chen and Zhang*, 2013; *Halverson et al*., 2006; *Durden*, 2013] others have argued against such a relation [*Stern and Nolan*, 2012; *Stern and Zhang*, 2013, 2016]. The arguments against a relationship between the warm-core structure and intensity invoke hydrostatic balance to show that it is only the integrated effect of the warm core, and not the details of its vertical structure (i.e., the altitude and number of temperature anomalies), which determines the surface pressure. However, this hydrostatic argument [see *Hirschberg and Fritsch*, 1993] basically assumes that the time tendency of the pressure field at some upper level is negligible, so that surface pressure tendencies are affected only by changes in the integrated warm-core temperature. Neglecting changes in the upper level pressure field is consistent with the *balanced vortex model* and its underlying assumptions. Relaxing this assumption, however, complicates the dynamics because the surface pressure tendency must then be deduced from the continuity equation and the net mass divergence in the column [*Steenburgh and Holton*, 1993].

The effects of upper level dynamics have been considered in numerous studies in the context of an externally generated upper level trough [i.e., *Kaplan and DeMaria*, 2003; *Molinari and Vollaro*, 1989, 1990; *Molinari et al*., 1995; *Montgomery and Farrell*, 1993; *Molinari et al*., 2004; *Peirano et al*., 2016]. *Emanuel and Rotunno* [2011] studied the nonexternal effect by examining the self-stratification of the outflow along angular momentum surfaces. Yet those branches of the circulation extend too far from the TC core to be hydrostatically related to the surface pressure anomaly at the center.

As explained above, under the assumption of gradient wind balance, the pressure gradients are decoupled from the radial flow at the upper levels and these two aspects of a TC can be studied separately. Thus, the warm-core structure is projected downward to yield the surface pressure variations, assuming that the upper level pressure gradients is insignificant. At the same time, a nontrivial upper level dynamic is considered mainly to result from an interaction of the TC with external synoptic features. Both of these essentially constrain the effect of the warm core on the upper level pressure field so that the latter will maintain gradient wind balance with the Coriolis and centrifugal forces.

While it is generally accepted that the warm core may generate a high-pressure center at the upper levels, it seems to be overlooked that around a high at the scale of a TC the gradient wind balance may be invalid. An invalidity of gradient wind balance (which may take place even with pressure gradients that are relatively small compared to values found at the level of maximum winds) recouples the radial pressure gradient and the radial velocity at the outflow level. Such coupling may yield self-induced upper level dynamics in TCs, which cannot be described by the balanced vortex model. The goal of this work is to examine the validity of gradient wind balance at the upper levels of simulated TCs in different physical configurations.

2. Definition of Gradient Nonbalance

In axisymmetric and pressure coordinates, gradient wind balance stems from the radial component of Newton's second law acting on an air parcel, assuming inviscid flow:

$$\frac{\partial u}{\partial t} + u\frac{\partial u}{\partial r} + \omega\frac{\partial u}{\partial p} = \underbrace{\frac{v^2}{r} + fv - g\frac{\partial Z}{\partial r}}_{\text{gradient balance}} \tag{1}$$

Here u and v are the radial and tangential winds, defined, respectively, as positive for outward and cyclonic flow (counterclockwise in the Northern Hemisphere), r is the radius, ω is the vertical velocity in pressure coordinates, Z is the geopotential height (the height of a given pressure surface), g is the gravitational acceleration

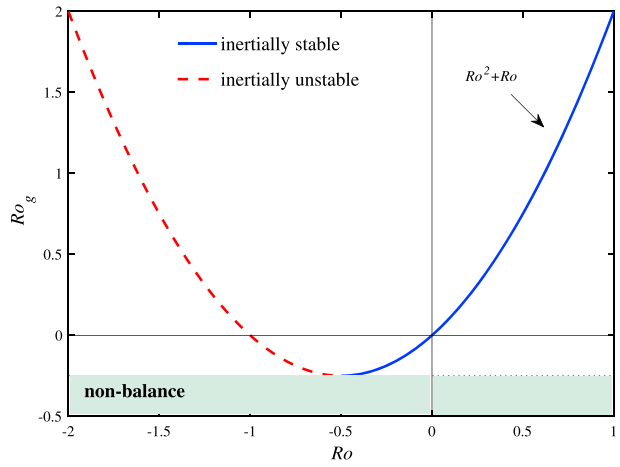

Figure 1. A canonical representation of the nondimensional gradient wind balance with *Ro* as the abscissa and Ro_g as the ordinate taken from *Cohen et al.* [2015]. Nonbalance as defined here occurs at values of $Ro_g < -¼$ in the light green area. The solid-blue and dashed-red parts of the curve represent parameter ranges of inertial stability ($Ro_g > -¼$; $-½ < Ro$) and possible inertial instability and imbalance ($Ro_g > -¼$; $Ro < -½$), respectively.

(assumed constant), f is the Coriolis parameter, and p is the pressure. Gradient wind balance is defined by the vanishing of the sum of forces on the right-hand side (RHS) of equation (1).

A nondimensional formulation is derived by assuming gradient wind balance and dividing the RHS of equation (1) by f^{2r} [*Cohen et al.*, 2015]:

$$Ro^2 + Ro = Ro_g. \qquad (2)$$

Here $Ro = v/fr$ is the Rossby number, $Ro_g = v_g/fr$ is the geostrophic Rossby number with $v_g = (g\partial Z/\partial r)/f$ as the geostrophic wind (defined to be negative around a high). Equation (2) classifies the possible solutions of the gradient wind balance around a high ($Ro_g < 0$) or a low ($Ro_g > 0$). In Figure 1 the left-hand side of (2) is plotted as a function of *Ro*, with Ro_g as a free parameter; for $Ro_g < -¼$ equation (2) has no solutions (see equation 3.16 in *Holton* [2004]). The common use of this plot is to classify the flow by the value of *Ro*, assuming it is a solution of gradient wind balance ($Ro_g \geq -¼$). Thus, one obtains the classification of the flow as inertially stable ($Ro > -½$) and inertially unstable ($Ro < -½$), with $Ro = -½$ marking zero absolute vorticity and the margin of stability (see *Cohen et al.* [2015] for details).

Here however, we examine the pressure map (Ro_g) rather than the wind (*Ro*). Around a low ($Ro_g > 0$) any combination of radii and pressure gradients (represented by Ro_g) can be balanced by a corresponding wind (*Ro*). Around a high ($Ro_g < 0$) equation (2) has no physical (mathematically real) solutions if $Ro_g < -¼$ (a strong enough pressure gradient and small enough radius) regardless of the wind (*Ro*). In terms of force balance, around a high (unlike around a low) the pressure gradient force and the centrifugal force both point outward. If the pressure gradient is strong enough and/or if the curvature is strong enough ($1/r$ is large), the Coriolis force cannot oppose the centrifugal and pressure gradient forces combined. Attempting to regain balance by increasing the velocity is futile as it will increase the outward pointing centrifugal force (v^2/r) more than the inward pointing Coriolis force (fv). We term such a scenario as *gradient nonbalance* to differentiate it from *gradient imbalance*. The latter arise due to friction, strong accelerations, and instability and may be eliminated (restoring balance) by a modification of the velocity to balance the pressure field.

One may think of nonbalance flow as analogues to the much more familiar scenario of nonhydrostatic flow. In the nonbalance flow, the radial pressure gradient is coupled with the radial velocity just as in a nonhydrostatic flow, the vertical pressure gradient is coupled with the vertical velocity.

The existence of a high above the warm core of TCs is expected from hydrostatic considerations if the warm anomaly is sufficiently strong and/or deep. Observations of the tops of TCs (around the 150 hPa pressure level) are rather rare. *Koteswaram* [1967] reported the formation of a split high at upper levels (~15 km in altitude), with two local maxima at a finite radius and a low at the center (see his Figure 16). *Halverson et al.* [2006] reported an example of the height of the tropopause having a dipole structure (see their Figure 11).

The balanced vortex model predicts an anticyclonic circulation when the angular momentum surface, flaring outward and upward from the radius of maximum wind (RMW, hereafter), reaches to sufficiently large radius. This anticyclonic circulation (and the high pressure inferred from it via gradient balance) has to be weak and wide to satisfy the $Ro_g \geq -1/4$ condition. As this absolute angular momentum

surface is also a moist saturated entropy surface [*Emanuel*, 1986] it bounds the warm core. Hydrostatically, additional heating in the warm core will generate a high about the scale of the RMW (see Figure S1 in the supporting information). At that scale, the $Ro_g \geq -1/4$ condition amounts to a remarkably small value of the pressure gradient (or geostrophic wind): assuming low latitudes ($f = 5 \times 10^{-5}$ s^{-1}) and a radial scale of 100 km, a relatively modest geostrophic wind speed of -5 m/s (negative by definition around a high) is already sufficient for significant nonbalance. This nonbalance recouples the radial pressure gradient and the radial velocity in equation (1). This makes the upper level dynamics in TCs important as it may generate excess mass divergence (beyond the value needed just to compensate for the low-level frictional convergence) and surface pressure tendencies, potentially leading to TC intensification. Subsequently, TC evolution may be sensitive to the structure of the high at its top (i.e., size and curvature, which determine the centrifugal force).

A simple understanding of the shapes of high-pressure structures can be obtained from a heuristic hydrostatic argument by assuming a simplified TC with a Gaussian-shaped lower level geopotential height field ($Z_{850\ \mathrm{hPa}}$) and Gaussian-shaped vertically mean temperature ($\overline{T}$) field between $Z_{850\ \mathrm{hPa}}$ and the upper level geopotential height ($Z_{150\ \mathrm{hPa}}$). We assume that $Z_{850\ \mathrm{hPa}}$ has a width $\sigma_Z = 70$ km and an amplitude of -200 m, and $\overline{T}$ has an amplitude of 4°C with width σ_T with values close to σ_Z (Figure 2a) and calculate the hydrostatic value of $Z_{150\ \mathrm{hPa}}$. The strong dependence of the $Z_{150\ \mathrm{hPa}}$ on the relative positioning (x_0) and width ratio (σ_T/σ_Z) is shown in Figures 2b–2i. The shape of the high at the top is highly sensitive to the offset ($x_0 \neq 0$) and/or widths ratio ($\sigma_T/\sigma_Z \neq 1$) with the former responsible for the asymmetry of the high (see Figures 2d and 2e) and the latter responsible for the annulus shape (see Figures 2f and 2g). An offset may result from the Earth's curvature (so-called "beta effect"), ambient wind shear, or other asymmetric environmental forcing. A width ratio ($\sigma_T/\sigma_Z > 1$) is implied by the slantwise moist neutrality which is a key aspect of the steady axisymmetric model [*Emanuel*, 1986] and results in a large outward slope of the TC eyewall [*Stern and Nolan*, 2009]. Such an annular shape high is implied by the radiosonde-based composite [*Koteswaram*, 1967]. A combination of offset and width difference is shown in Figures 2h and 2i.

The case with $x_0 = 0$ and $\sigma_T = \sigma_Z$ in Figures 2b and 2c has small value of nonbalance. The complex high-pressure centers in Figures 2d–2i have much stronger curvature leading to an order of magnitude increase in nonbalance. Thus, some of the aforementioned observations may contradict the balanced vortex model (at least in those certain instances and locations). Since high-altitude observations are rare, it is not clear whether such nonbalance conditions are ubiquitous in real TCs and how TCs readjust to balanced flow if any of the above mentioned conditions occur.

3. Simulated TCs and Data Analysis

We examine the validity of the gradient wind balance in the upper level pressure maps of 12 TC simulations, taken from different studies [*Nolan et al.*, 2013; *Zhang and Tao*, 2013; *Zhang and Weng*, 2015; *Weng and Zhang*, 2016; *Emanuel and Zhang*, 2017]. All the simulations were performed using the Advanced Research version of the Weather, Research, and Forecasting (WRF) model (see supporting information for details).

The relevant outputs from the WRF model are the geopotential height, pressure, potential temperature, water mixing ratio, and 3-D velocity components on surfaces of constant $\eta = (p - p_t)/(p_s - p_t)$. Here p is the hydrostatic pressure while p_t and p_s are its values at the model top and surface, respectively; see section 2.1 in *Skamarock et al.* [2008] for details. In order to calculate the horizontal components of the pressure gradient force (and thus the geostrophic wind) we interpolated these variables to constant pressure surfaces using a quadratic interpolation from η to log-pressure (all storms are analyzed over the ocean which circumvents issues of topography). For clarity we eliminate noisy small-scale features by averaging the WRF data, taking 6-hourly time means and 9 km horizontal means.

We focus only on the axisymmetric mean structure of the storms and leave the asymmetric aspects for future studies. The axisymmetric mean is calculated about the storm's center (location of minimum 850 hPa geopotential height) in the pressure-interpolated fields. It is assumed here that f at the storm center represents its value over the entire central region of the storm. In the axisymmetric and pressure coordinate, the radial gradient of the geopotential height (Z) over f provides the geostrophic wind (v_g) while the radial distance from the center defines the radius of curvature (r) for the calculation of $Ro_g = v_g/fr$.

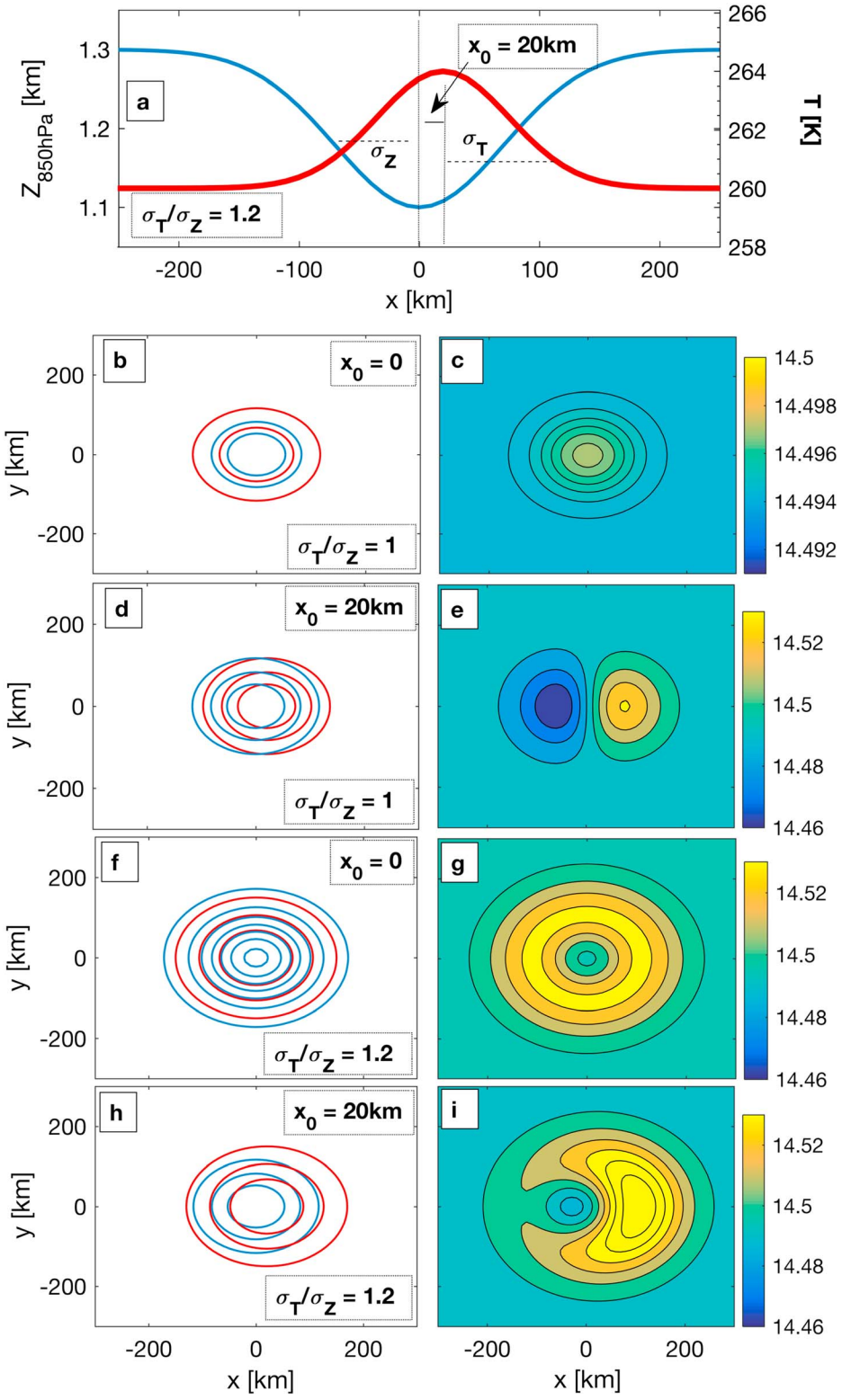

Figure 2. The upper level geopotential height ($Z_{150\ m}$) as a hydrostatic sum of a Gaussian shape low ($Z_{850\ hPa}$) and a Gaussian shape vertically mean temperature ($\overline{T}$) for several cases. (a) The cross section of the $Z_{850\ hPa}$ Gaussian (blue, with minimum 200 m lower than ambient value) and $\overline{T}$ Gaussian (red, with maximum 4 K higher then ambient value). In this case the latter Gaussian is 28% wider (σ_T/σ_Z = 1.28) and horizontally offset by 20 km (x_0). (b, d, f, and h) The contours of $Z_{850\ hPa}$ (blue) and $\overline{T}$ (red) for x_0 = 0, σ_T/σ_Z = 1; x_0 = 20 km, σ_T/σ_Z = 1; x_0 = 0, σ_T/σ_Z = 1.28; x_0 = 20 km, σ_T/σ_Z = 1.28, respectively. (c, e, g, and i) The $Z_{150\ hPa}$ as their hydrostatic sum in kilometers.

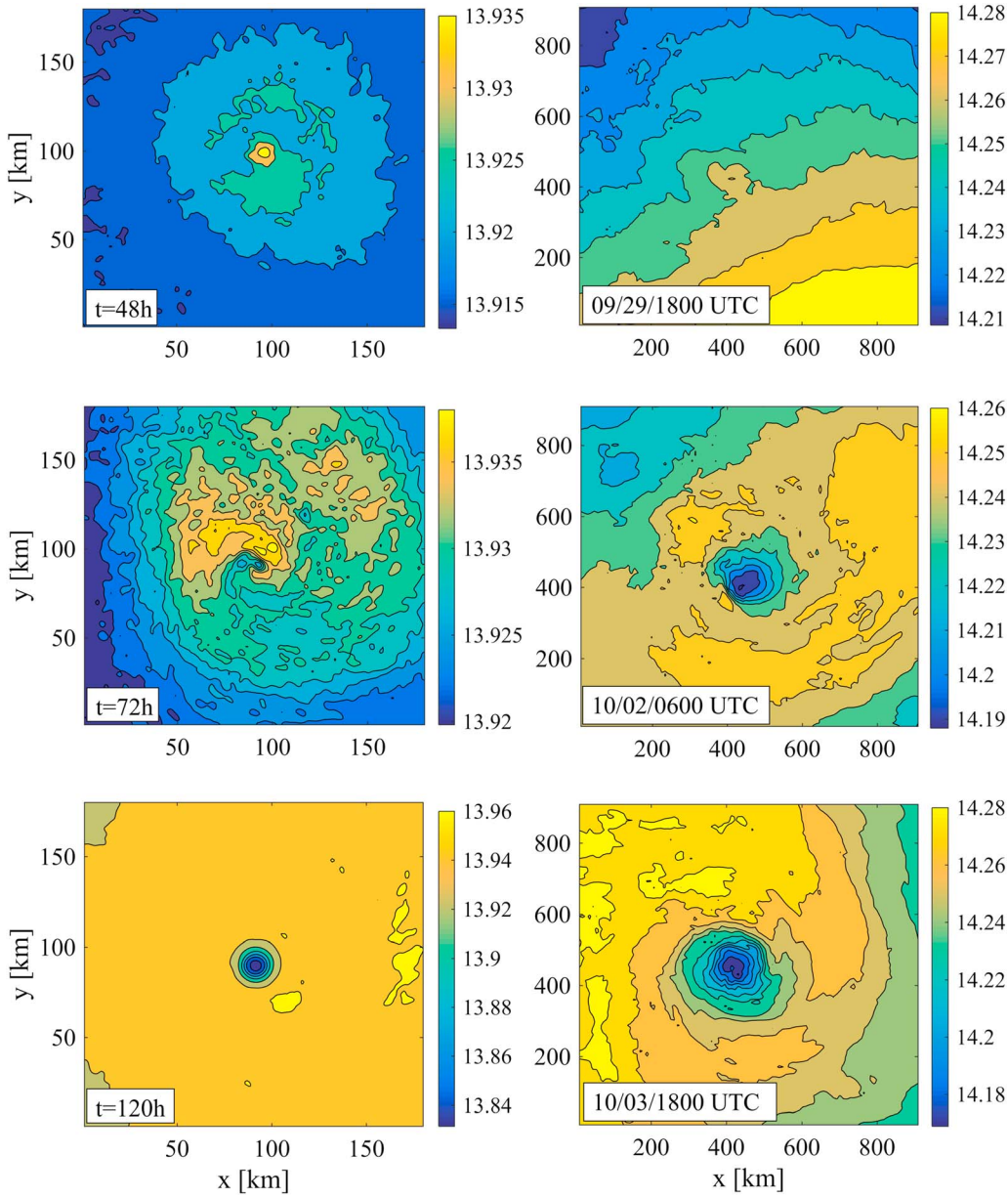

Figure 3. The 150 hPa geopotential height field (in km) in two different simulations (columns) and at three different times (rows). The left column is INR with time marking hours from the start of the simulation. The right column is simulated Joaquin 2015 at three different times.

In order to produce an index that quantifies the nonbalance state in the axisymmetric mean we radially integrate Ro_g at the 150 hPa. Since the parts in the Ro_g profile that can be balanced ($Ro_g \geq -1/4$) do not cancel out with nonbalanced parts ($Ro_g < -1/4$) we eliminate the former by defining this index as follows:

$$\Lambda = \frac{1}{{r_1}^2} \int_0^{r_1} \left(\frac{X}{2} [\mathrm{sgn}(X) + 1] \right) r dr \tag{3}$$

Here $X = -(Ro_g + 1/4)$ so that positive X corresponds to nonbalance, while the integration domain, r_1, is taken to be three times RMW. This positive index, Λ, reflects the accumulated magnitude of the nonbalance normalized by the storm size and $\Lambda = 0$ corresponds to potentially balanced flow.

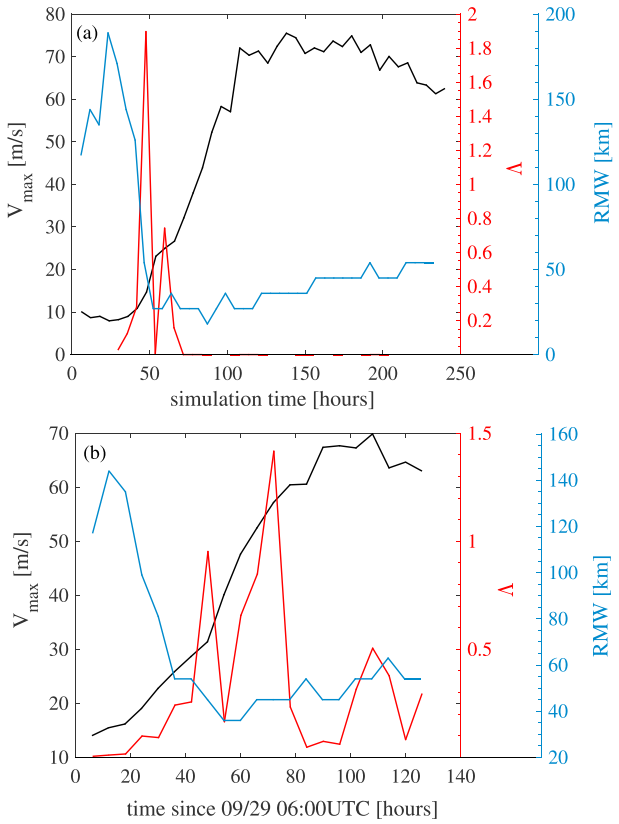

Figure 4. (a and b) INR and Joaquin 2015, respectively. Here the time evolution of V_{max} (black, that corresponds to the left ordinate), the nonbalance index $-\Lambda$ (red, corresponding to the intermediate ordinate on the right) and RMW (blue, corresponding to the right most ordinate) are shown.

4. Results

Figure 3 shows the 150 hPa geopotential height (km) in the idealized TC simulation on the *f* plane (INR, storm number 6 in Table S2) and in a real-case TC simulation TC (Joaquin 2015, storm number 11 in Table S2) [*Weng and Zhang*, 2016; *Emanuel and Zhang*, 2017]. These geopotential height maps are shown for three different times during the life of the TC, and in both cases a high pressure develops and eventually decays. Such high-pressure centers entail nonbalance in both cases. Figure 4 shows the value of Λ along with the storms' maximum tangential wind (V_{max}) and RMW. Figures 4a and 4b show the temporal evolution of these three parameters in the simulations shown in Figures 3a and 3b, respectively. Both storms experience a drastic contraction of the RMW followed by a moderate and slow increase in RMW. As reported by *Stern et al.* [2015] this contraction is accompanied by a moderate intensification and is directly followed by a stronger intensification before peak intensity is achieved. With this temporal evolution in mind we note that nonbalance (Λ) peaks toward the end (or following) the contraction stage and diminishes at later intensification stages. This peak of nonbalance during intensification is found in all 12 TC simulations used in this study; however, its exact timing may differ between simulations. Moreover, storms simulated on the *f* plane regain complete balance ($\Lambda = 0$) when both the intensification and contraction have tapered off (typically after several simulation days). However, storms simulated on the sphere do not regain complete balance during their simulation time.

This suggests that Λ is a proxy for TC intensity. Figure 5a compares the 24 h mean Λ (ordinate) and V_{max} (abscissa) for all days in the 12 simulations examined in this study with the values at the time of maximum Λ for each storm shown in large dots. Figure 5b shows the correlation between the total intensification (the difference between the maximum and the minimum values of V_{max}) and the cumulative nonbalance (lifecycle sum of Λ) for these 12 storms. Note that we analyze the 6 h mean of the model output which removes the possible effects of different time stepping. Moreover, since Λ diminishes (or vanishes) after significant intensification is completed the simulation's length does not contribute to the sum of Λ. In both panels the correlation was calculated excluding the outlier (red dot). Examining the time development of the various storms by looking at plots like those shown in Figure 4 for all 12 cases (not shown) finds that nonbalance events take place during (and often at the onset) of a significant intensity increase, although it is not necessary for intensification to occur following each nonbalance event.

5. Discussion

This work examines the validity of gradient wind balance, which is assumed in many theories of TC structure and evolution. Previous studies have reexamined the precision of the wind predicted by the gradient wind balance and the importance of imbalance [e.g., *Bryan and Rotunno*, 2009] which occurs at most stages of

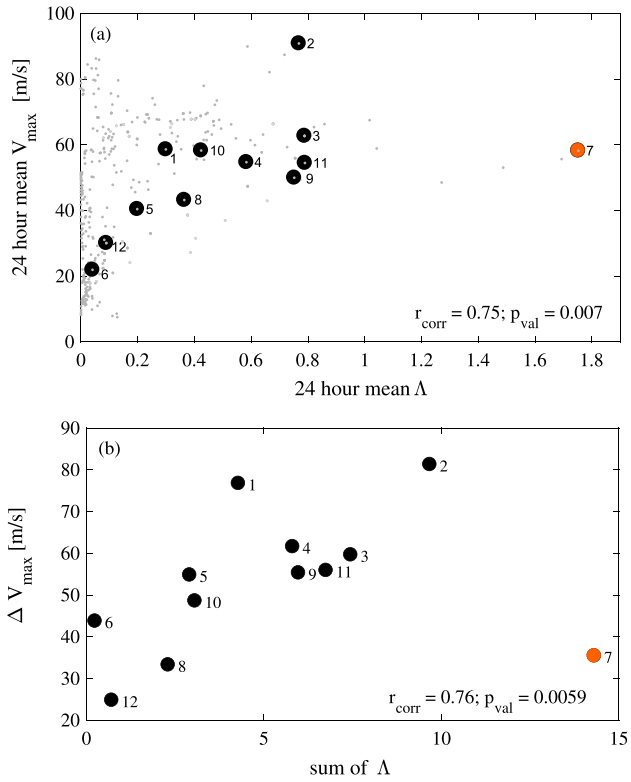

Figure 5. (a) Scatterplot of the 24 h mean V_{max} and its corresponding 24 h mean Λ for all storms (small gray dots) with the large dots indicating these values at the time of maximum (24 h mean) of Λ per storm. (b) Scatterplot of the intensity change during the entire simulation (difference between the maximum and the minimum values of V_{max}) as a function of sum of Λ for the same storms. In both figures the numbers correspond to the simulation numbers shown in Table S2 in the supporting information. The coefficients of a linear correlation were calculated after removing the outlier in red (which is a real-time simulation of Earl2010).

the storm. However, here we examine a different case in which gradient wind balance cannot be a solution of the radial momentum equation given a specific pressure field. This nonbalance occurs mostly in the early stages of intensification that is associated with contraction of the RMW [*Stern et al.*, 2015], while in the later stages of the storm's life which has nearly constant RMW the gradient wind balance has valid solutions for the pressure field.

Even though a correlation is found between certain aspects of nonbalance and intensification, the questions of causation should be further explored, possibly by designing WRF simulations that facilitate a clear comparison between storms. For instance, since TCs in nature have a wide variety of sizes (RMW) and $Ro_g \sim 1/r$, nonbalance is more likely in smaller storms.

The assumption of gradient wind balance throughout the TC relies on a rapid adjustment mechanism toward balance at every level. In the lower and middle levels of a TC, where the flow is around a low, deviations from this balance (gradient imbalance) may be dynamically adjusted by modifying the wind speed to a new value that is in gradient wind balance with the pressure field (while conserving absolute angular momentum). In the case of nonbalance however, a modification of the pressure field is required in order to restore balance, which is nontrivial.

In the classical description of TC [*Emanuel*, 1986] surfaces of absolute angular momentum dynamically link the upper levels of the storm to their corresponding values at the top of the boundary layer. The outward flaring of these lines predicts that the area of the inner core of the storm (which is defined in lower levels as the area inward from the radius of maximum winds) will increase with altitude. Thus, at the 150 hPa level (about 15 km) a larger portion of the storm, including the areas of nonbalance described here, is essentially linked to the dynamics of the eye, where the gradient balance is not necessarily a valid assumption [*Smith*, 1980].

It is left for future work to assess the effects of enforcing gradient wind balance in a model (i.e., decoupling the two sides of equation (1)) on the net divergence in a column. This assumption could be equivalent to assuming instantaneous adjustment of the pressure field (and thus the warm core) to values allowed by the gradient wind balance and might underestimate upper level divergence, and thus underestimating surface pressure changes.

The annular shape of the upper level high depicted in Figures 2g and 2i is consistent with the observational findings summarized in Figure 16a in *Koteswaram* [1967]. This structure implies a maximum nonbalance (and thus divergence) at a finite radius from the center with down-gradient flows outward as well as to the center at the upper levels. If true, such convergence at the center top and a descending motion at the center would

be consistent with the circulation observed in the eye of TCs. However, the annular high found in these few observations is narrow compared with that found in high-resolution WRF simulations. There is a need for more detailed upper level observations at altitudes around 15 km (150 hPa) in order to examine the existence of nonbalance and its impacts. The recent Tropical Cyclone Intensity observational campaign [e.g., *Rogers et al*., 2017], which was aimed at the upper levels of TCs, is promising in this regard.

Acknowledgments
The work was supported by the Israeli Science Foundation grant 1537/12. Part of the work was done during the sabbatical of NH at Stockholm University, supported by a Rossby Visiting Fellowship from the International Meteorological Institute of Stockholm University. F.Z. and D.T. are partially supported by the Office of Naval Research (grant N000140910526) and the Hurricane and Severe Storm Sentinel (HS3) investigation under NASA's Earth Venture Program and NOAA's Hurricane Forecast Improvement Program (HFIP). D.N. is supported by NASA CloudSat Program through grant NNX16AP19G. We thank Yonghui Weng for performing the real-world TC simulations used in this study, and the Texas Advanced Computing Center (TACC) for the computing. The Hurricane Nature Run simulation was performed at the Center for Computing Sciences at the University of Miami. Useful comments from both T. Cronin and from another, anonymous, reviewer greatly contributed to the final form of this work.

References

Bryan, G. H., and R. Rotunno (2009), Evaluation of an analytical model for the maximum intensity of tropical cyclones, *J. Atmos. Sci.*, *66*(10), 3042–3060.
Charney, J. G., and A. Eliassen (1964), On the growth of the hurricane depression, *J. Atmos. Sci.*, *21*(1), 68–75.
Chen, H., and D. L. Zhang (2013), On the rapid intensification of Hurricane Wilma (2005). Part II: Convective bursts and the upper-level warm core, *J. Atmos. Sci.*, *70*(1), 146–162.
Durden, S. L. (2013), Observed tropical cyclone eye thermal anomaly profiles extending above 300 hPa, *Mon. Weather Rev.*, *141*(12), 4256–4268.
Cohen, Y., Y. Dvorkin, and N. Paldor (2015), Linear instability of warm core, constant potential vorticity, eddies in a two-layer ocean, *Q. J. R. Meteorol. Soc.*, *141*, 1884–1893.
Eliassen, A. (1951), Slow thermally or frictionally controlled meridional circulation in a circular vortex, *Astrophys. Norv.*, *5*, 19.
Emanuel, K. A. (1986), An air-sea interaction theory for tropical cyclones. Part I: Steady-state maintenance, *J. Atmos. Sci.*, *43*(6), 585–605.
Emanuel, K. A. (1995), Sensitivity of tropical cyclones to surface exchange coefficients and a revised steady-state model incorporating eye dynamics, *J. Atmos. Sci.*, *52*(22), 3639–3976.
Emanuel, K., and R. Rotunno (2011), Self-stratification of tropical cyclone outflow. Part I: Implications for storm structure, *J. Atmos. Sci.*, *68*(10), 2236–2249.
Emanuel, K., and F. Zhang (2017), The role of inner core moisture in tropical cyclone predictability and practical forecast skill, *J. Atmos. Sci.*, *74*, 2315–2324, doi:10.1175/JAS-D-17-0008.1.
Halverson, J. B., J. Simpson, G. Heymsfield, H. Pierce, T. Hock, and L. Ritchie (2006), Warm core structure of Hurricane Erin diagnosed from high altitude dropsondes during CAMEX-4, *J. Atmos. Sci.*, *63*(1), 309–324.
Hirschberg, P. A., and J. M. Fritsch (1993), On understanding height tendency, *Mon. Weather Rev.*, *121*(9), 2646–2661.
Holton, J. R. (2004), *An Introduction to Dynamic Meteorology*, 4th ed., Elsevier Acad. Press, New York.
Kaplan, J., and M. DeMaria (2003), Large-scale characteristics of rapidly intensifying tropical cyclones in the North Atlantic basin, *Weather Forecasting*, *18*(6), 1093–1108.
Koteswaram, P. (1967), On the structure of hurricanes in the upper troposphere and lower stratosphere, *Mon. Weather Rev.*, *95*(8), 541–564.
Molinari, J., and D. Vollaro (1989), External influences on hurricane intensity. Part I: Outflow layer eddy angular momentum fluxes, *J. Atmos. Sci.*, *46*(8), 1093–1105.
Molinari, J., and D. Vollaro (1990), External influences on hurricane intensity. Part II: Vertical structure and response of the hurricane vortex, *J. Atmos. Sci.*, *47*(15), 1902–1918.
Molinari, J., S. Skubis, and D. Vollaro (1995), External influences on hurricane intensity. Part III: Potential vorticity structure, *J. Atmos. Sci.*, *52*, 3593–3606.
Molinari, J., D. Vollaro, and K. L. Corbosiero (2004), Tropical cyclone formation in a sheared environment: A case study, *J. Atmos. Sci.*, *61*(21), 2493–2509.
Montgomery, M. T., and B. F. Farrell (1993), Tropical cyclone formation, *J. Atmos. Sci.*, *50*(2), 285–310.
National Hurricane Center (2010), Hurricane Igor discussion number 40. [Available at http://www.nhc.noaa.gov/archive/2010/al11/al112010.discus.040.shtml.]
Nolan, D. S., Y. Moon, and D. P. Stern (2007), Tropical cyclone intensification from asymmetric convection: Energetics and efficiency, *J. Atmos. Sci.*, *64*(10), 3377–3405.
Nolan, D. S., R. Atlas, K. T. Bhatia, and L. R. Bucci (2013), Development and validation of a hurricane nature run using the joint OSSE nature run and the WRF model, *J. Adv. Model. Earth Syst.*, *5*(2), 382–405.
Ohno, T., and M. Satoh (2015), On the warm core of a tropical cyclone formed near the tropopause, *J. Atmos. Sci.*, *72*(2), 551–571.
Ooyama, K. (1969), Numerical simulation of the life cycle of tropical cyclones, *J. Atmos. Sci.*, *26*(1), 3–40.
Ooyama, K. V. (1982), Conceptual evolution of the theory and modeling of the tropical cyclone, *J. Meteor. Soc. Jpn.*, *60*(1), 369–380.
Peirano, C. M., K. L. Corbosiero, and B. H. Tang (2016), Revisiting trough interactions and tropical cyclone intensity change, *Geophys. Res. Lett.*, *43*, 5509–5515, doi:10.1002/2016GL069040.
Raymond, D., Z. Fuchs, S. Gjorgjievska, and S. Sessions (2015), Balanced dynamics and convection in the tropical troposphere, *J. Adv. Model. Earth Syst.*, *7*, 1093–1116, doi:10.1002/2015MS000467.
Rodgers, R., S. Aberson, D. Cecil, J. Doyle, J. Morgerman, T. Kimberlain, L. K. Shay, and C. Velden (2017), Re-writing the tropical record books: The extraordinary intensification of Hurricane Patricia (2015), *Bull. Am. Meteorol. Soc.*, doi:10.1175/BAMS-D-16-0039.1.
Shapiro, L. J., and H. E. Willoughby (1982), The response of balanced hurricanes to local sources of heat and momentum, *J. Atmos. Sci.*, *39*, 378–394.
Skamarock, W.C., Klemp, J.B., Dudhia, J., Gill, O. D., Barker, D. M., Duda, M. G. Huang, X., Wang, W. and J. G. Powers (2008), A description of the advanced research WRF version 3, tech. Note, NCAR/TN-475+STR, Natl. Cent. for Atmos. Res., Boulder, Colo.
Smith, R. K. (1980), Tropical cyclone eye dynamics, *J. Atmos. Sci.*, *37*, 1227–1232.
Steenburgh, W. J., and J. R. Holton (1993), On the interpretation of geopotential height tendency equations, *Mon. Weather Rev.*, *121*(9), 2642–2645.
Stern, D. P., and D. S. Nolan (2009), Reexamining the vertical structure of tangential winds in tropical cyclones: Observations and theory, *J. Atmos. Sci.*, *66*(12), 3579–3600.
Stern, D. P., and D. S. Nolan (2012), On the height of the warm core in tropical cyclones, *J. Atmos. Sci.*, *69*(5), 1657–1680.
Stern, D. P., and F. Zhang (2013), How does the eye warm? Part I: A potential temperature budget analysis of an idealized tropical cyclone, *J. Atmos. Sci.*, *70*(1), 73–90.
Stern, D. P., and F. Zhang (2016), The warm core structure of Hurricane Earl (2010), *J. Atmos. Sci.*, *73*, 3305–3328.

Stern, D. P., D. S. Nolan, and F. Zhang (2015), Revisiting the relationship between eyewall contraction and intensification, *J. Atmos. Sci.*, *72*, 1283–1206.
Weng, Y., and F. Zhang (2016), Advances in convection-permitting tropical cyclone analysis and prediction through EnKF assimilation of reconnaissance aircraft observations, *J. Meteor. Soc. Jpn.*, *94*, 345–358.
Willoughby, H. E. (1990), Gradient balance in tropical cyclones, *J. Atmos. Sci.*, *47*, 225–274.
Wirth, V., and T. J. Dunkerton (2009), The dynamics of eye formation and maintenance in axisymmetric diabatic vortices, *J. Atmos. Sci.*, *66*(12), 3601–3620.
Zhang, F., and D. Tao (2013), Effects of vertical wind shear on the predictability of tropical cyclones, *J. Atmos. Sci.*, *70*(3), 975–983.
Zhang, F., and Y. Weng (2015), Predicting hurricane intensity and associated hazards: A five-year real-time forecast experiment with assimilation of airborne Doppler radar observations, *Bull. Am. Meteorol. Soc.*, *96*(1), 25–33.